

# Spectroscopic Signatures for Interlayer Coupling in MoS<sub>2</sub>-WSe<sub>2</sub> van der Waals Stacking

Ming-Hui Chiu,<sup>#^</sup> Ming-Yang Li,<sup>¶^</sup> Wengjing Zhang,<sup>%</sup> Wei-Ting Hsu,<sup>&</sup> Wen-Hao Chang,<sup>&</sup> Mauricio Terrones,<sup>+</sup> Humberto Terrones,<sup>§</sup> and Lain-Jong Li<sup>#\*</sup>

<sup>#</sup>*Physical Sciences and Engineering, King Abdullah University of Science and Technology, Thuwal, 23955-6900, Kingdom of Saudi Arabia.*

<sup>¶</sup>*Institute of Atomic and Molecular Sciences, Academia Sinica, Taipei, 11529, Taiwan.*

<sup>%</sup>*Department of Physics, National University of Singapore, 2 Science Drive 3, Singapore 117542. SZU-NUS Collaborative Innovation Center for Optoelectronic Science & Technology, Shenzhen University, Shenzhen 518060, China*

<sup>&</sup>*Department of Electrophysics, National Chiao Tung University, Hsinchu, 300 Taiwan*

<sup>+</sup>*Department of Physics, Chemistry, Materials Science and Engineering and Center for 2-Dimensional and Layered Materials, 104 Davey Lab., The Pennsylvania State University, University Park, Pennsylvania, 16802, United States*

<sup>§</sup>*Department of Physics, Applied Physics and Astronomy, Rensselaer Polytechnic Institute, 110 Eighth Street, Troy 12180, USA.*

<sup>^</sup> These authors contributed equally.

<sup>\*</sup> To whom correspondence should be addressed: (L. J. Li) [lance.li@kaust.edu.sa](mailto:lance.li@kaust.edu.sa)

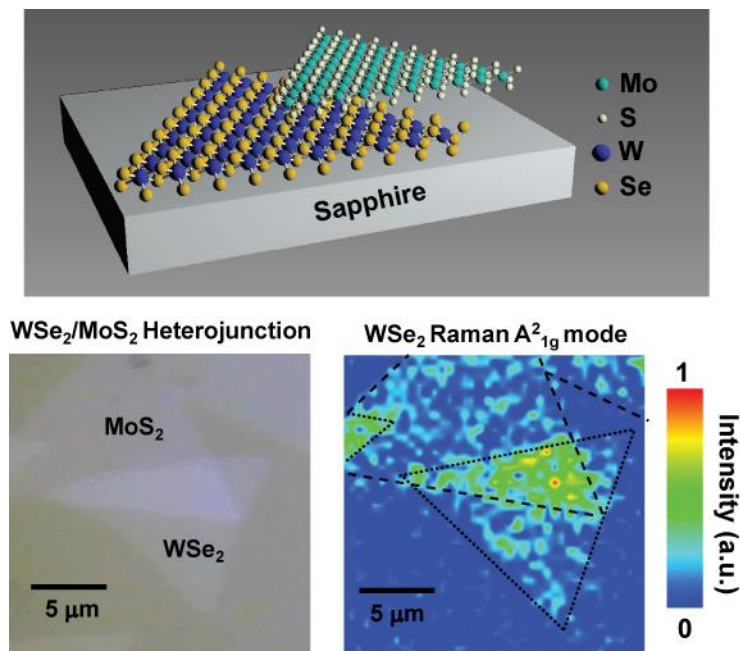
**KEYWORDS:** Transition metal dichalcogenides; Tungsten diselenides; Molybdenum disulfide; Van der Waals stacking; Hetero-junction; Inter-layer coupling.

**BRIEFS:** We report the Raman and PL spectroscopic signatures for the interlayer coupling between MoS<sub>2</sub> and WSe<sub>2</sub> monolayers in their van der Waals stacking.

## ABSTRACT

Stacking of MoS<sub>2</sub> and WSe<sub>2</sub> monolayers is conducted by transferring triangular MoS<sub>2</sub> monolayers on top of WSe<sub>2</sub> monolayers; all grown by chemical vapor deposition (CVD). Raman spectroscopy and photoluminescence (PL) studies reveal that these mechanically stacked monolayers are not closely coupled but after a thermal treatment at 300°C, it is possible to produce novel van der Waals solids consisting of two interacting transition metal dichalcogenide (TMD) monolayers. The layer-number sensitive Raman out-of-plane mode A<sup>2</sup><sub>1g</sub> for WSe<sub>2</sub> (309 cm<sup>-1</sup>) is found sensitive to the coupling between two TMD monolayers. The presence of interlayer excitonic emissions and the changes in other intrinsic Raman modes such as E<sup>2</sup>′ for MoS<sub>2</sub> at 286 cm<sup>-1</sup> and A<sup>2</sup><sub>1g</sub> for MoS<sub>2</sub> at around 463 cm<sup>-1</sup> confirm the enhancement of the interlayer coupling.

## Table of Content



Semiconducting transition metal dichalcogenide (STMD) layered materials exhibit unique layer-dependent electronic and optical properties.<sup>1-12</sup> For example, molybdenum disulphide (MoS<sub>2</sub>) exhibits an indirect bandgap of 1.2 eV in bulk, but it becomes a direct gap semiconductor (bandgap = 1.8 eV) when thinned to a monolayer.<sup>4, 8</sup> Hence, monolayer MoS<sub>2</sub> transistors have been fabricated and these devices have showed excellent current on/off ratios.<sup>10-12</sup> MoS<sub>2</sub> is known as an *n*-type semiconductor due to the presence of S vacancies. Another STMD, tungsten diselenide (WSe<sub>2</sub>), has just started to attract the attention of numerous scientists due to its *p*-type characteristics.<sup>2, 13</sup> In addition to the mechanical exfoliation method to prepare STMD layers, recent developments in the scalable synthesis of STMD monolayers using chemical vapor deposition (CVD) opened up the possibility to form large area of STMD monolayers that could result in fabrication of flexible electronic devices and photodetectors.<sup>1, 2, 14</sup> Furthermore, it is also possible to envisage building unprecedented solids by stacking monolayers of different 2-D systems one on top of another (e.g. TMDs, h-BN and graphene).<sup>15-21</sup> Such stacked heterostructures based on atomically thin 2D layers are fundamentally different since only van der Waals interactions exist at the interfaces. Therefore, these layered materials (termed also van der Waals solids) enable the preparation of high-quality heterointerfaces without the need of fulfilling an atomic commensurability<sup>17, 18, 22</sup>, thus making the structure construction easily achievable. Very recently, MoSe<sub>2</sub>/WSe<sub>2</sub> optical studies were performed<sup>23</sup>, and other optoelectronic devices based on WSe<sub>2</sub>/MoS<sub>2</sub> *p-n* junction were also proposed.<sup>24-27</sup> Interestingly, the gate-tunable diode-like current rectification and a photovoltaic response have been recently observed in WSe<sub>2</sub>/MoS<sub>2</sub> heterojunctions.<sup>24-26</sup> It should be noted that the optical and electrical properties of TMD heterojunctions strongly depend on the interaction among layers, and efforts aiming at elucidating their proper characterization is currently underway.

In this paper, we demonstrate that it is possible to build novel van der Waals solids by first stacking CVD-grown MoS<sub>2</sub> on WSe<sub>2</sub> monolayers, followed by thermal annealing. The layer-number sensitive Raman mode A<sup>2</sup><sub>1g</sub> for WSe<sub>2</sub> at around 309 cm<sup>-1</sup> (out-of-plane mode) appears to be excellent parameters when evaluating a good coupling between monolayers. The Raman modes for bulk MoS<sub>2</sub> at *ca.* 463 cm<sup>-1</sup> (A<sup>2</sup><sub>1g</sub>) and at *ca.* 283 cm<sup>-1</sup> (E'') are also enhanced by interlayer coupling. In addition, the interlayer excitonic peak observed in photoluminescence (PL) confirms the coupling between two

TMD monolayers and a band diagram of the MoS<sub>2</sub>/WSe<sub>2</sub> heterojunction and the exciton binding energies for each composition are proposed.

## RESULTS AND DISCUSSIONS

***Preparation and Characterizations of Hetero-Junction:*** Triangular WSe<sub>2</sub> and MoS<sub>2</sub> single crystalline monolayers with the lateral dimension of few tens of micrometers were synthesized on c-plane sapphire substrates by CVD.<sup>1,2</sup> In brief, transition metal trioxides (MoO<sub>3</sub> or WO<sub>3</sub>) were vaporized and reacted with the S or Se vapor in a hot-wall furnace under a controlled gaseous environment to form MoS<sub>2</sub> or WSe<sub>2</sub> monolayers (see details in Experimental Methods). In order to build a van der Waals solid (or vertical hetero-junction of MoS<sub>2</sub> on WSe<sub>2</sub>), as schematically illustrated in Figure 1(a), we first detached as-synthesized MoS<sub>2</sub> triangular islands using PMMA. In particular, a layer of PMMA was spin-coated on MoS<sub>2</sub> followed by dipping it in NaOH so as to release the PMMA-supported MoS<sub>2</sub> from the substrates. The PMMA supported-MoS<sub>2</sub> was then mechanically transferred onto WSe<sub>2</sub> flakes followed by the removal/cleaning of PMMA.<sup>3</sup> Figure 1(b) is the optical micrograph (OM) showing the mechanically stacked MoS<sub>2</sub>/WSe<sub>2</sub> monolayers, in which it is possible to distinguish the stacked layers by noticing a color contrast. Supporting Figure S1 shows the atomic force microscopy (AFM) image of as-transferred MoS<sub>2</sub>/WSe<sub>2</sub>, where the surface of the sample is covered with residuals and adsorbates. In this context, it has been demonstrated by scanning tunneling microscopy (STM) that the majority of the adsorbates and residuals can be removed after thermal annealing at elevated temperatures.<sup>28</sup> Therefore, as-prepared MoS<sub>2</sub>/WSe<sub>2</sub> samples were then annealed in an hydrogen/Ar environment (atmosphere pressure; H<sub>2</sub>:Ar = 1:4) at 300°C for 4hr. The detailed fabrication process is described in the Experimental Methods.

The AFM image and cross-sectional profile of the MoS<sub>2</sub>/WSe<sub>2</sub> hetero-junction are shown in Figure 1(c), demonstrating that both WSe<sub>2</sub> and MoS<sub>2</sub> are indeed monolayers (thickness for each is around 0.6 ~ 0.7 nm). The AFM image also shows that the individual flakes are clean and without cracks or holes after the H<sub>2</sub>/Ar thermal treatment. Interestingly, the corrugated structures are found at the overlapped region, which could be due to a commensurability adjustment of the layers in order to

minimize the energy followed the thermal treatment. Alternatively, it is also possible that water, used as the solvent to transfer MoS<sub>2</sub> onto WSe<sub>2</sub>, got trapped between MoS<sub>2</sub> and WSe<sub>2</sub> monolayers, and its evaporation resulted in the corrugation of the top transferred layer during the thermal treatment. The high spikes of the cross-sectional profile in inset of Figure 1(c) reveal the profile of the corrugated structures.

**Raman Features:** For the Raman spectra we have used the notation of the monolayer modes using the symbols A<sub>1</sub>' , E' , and the notation of the bilayer for the higher order out of plane modes such as the A<sup>2</sup><sub>1g</sub> , since these modes are not Raman active in the monolayer. Figures 2(a) to 2(d) show the Raman spectra of the double layer van der Waals solid excited with a 473 nm laser in four energy regions, where the curves from the top to bottom are MoS<sub>2</sub> region (blue), MoS<sub>2</sub>/WSe<sub>2</sub> hetero-junction before annealing (green; uM/W), MoS<sub>2</sub>/WSe<sub>2</sub> hetero-junction after annealing (red; cM/W), and WSe<sub>2</sub> region (black), respectively. The characteristic peaks for WSe<sub>2</sub> at about 250 cm<sup>-1</sup> (E' and A<sub>1</sub>' degenerated mode) and those for MoS<sub>2</sub> located at 387 cm<sup>-1</sup> (E' mode; in-plane vibration) and 402 cm<sup>-1</sup> (A<sub>1</sub>' mode; out-of-plane vibration) are observed in individual monolayers of WSe<sub>2</sub> and MoS<sub>2</sub>. In addition, the layer-number sensitive mode A<sup>2</sup><sub>1g</sub> for WSe<sub>2</sub> at around 309 cm<sup>-1</sup> (out-of-plane mode) has been reported only observable when the WSe<sub>2</sub> is a bilayer or thicker.<sup>29, 30</sup> A similar feature A<sup>2</sup><sub>1g</sub> for bulk MoS<sub>2</sub> is located at around 463 cm<sup>-1</sup>.<sup>31-36</sup> Furthermore, there is another characteristic peak for bulk MoS<sub>2</sub> at around 284 cm<sup>-1</sup> in odd number of layers is called E'' and in even number of layers becomes E<sub>g</sub> due to the symmetry involved.<sup>31-33</sup> Our Raman results for either MoS<sub>2</sub> or WSe<sub>2</sub> region do not exhibit these characteristic peaks, confirming that WSe<sub>2</sub> and MoS<sub>2</sub> are monolayers. Note that the Raman band at 260 cm<sup>-1</sup> observed at WSe<sub>2</sub> region (Figures 2(a)) and at about 450 cm<sup>-1</sup> at MoS<sub>2</sub> region (Figures 2(d)) are corresponding to the second order LA(M) phonon (2LA(M)).<sup>35-37</sup>

It is observed that the Raman peaks for either MoS<sub>2</sub> or WSe<sub>2</sub> region show no obvious change after the thermal annealing at 300°C as shown in Figure S2(a), which implies that the annealing process does not cause significant structural defects or modification. For the hetero-junction before annealing, we find that the Raman characteristic peaks are closely coinciding with the individual WSe<sub>2</sub> and MoS<sub>2</sub> regions, which implies that the layers are un-coupled (independent from each other). By

contrast, after the thermal annealing process, the Raman spectrum for the hetero-junction becomes significantly different from those for the individual WSe<sub>2</sub> and MoS<sub>2</sub> monolayers. First, the layer-sensitive characteristic peak A<sup>2</sup><sub>1g</sub> for WSe<sub>2</sub> at 309 cm<sup>-1</sup> clearly appear in Figure 2(b). Secondly, the E' and A'<sub>1</sub> degenerated peak for the WSe<sub>2</sub> shows a blue-shift as shown in Figure 2(a), and the A'<sub>1</sub> (E') for the MoS<sub>2</sub> shows blue (red)-shifts as shown in Figure 2(c), respectively. Thirdly, the anomaly E'' feature for MoS<sub>2</sub> is also observed in Figure 2(b), and the layer-sensitive peak A<sup>2</sup><sub>1g</sub> for MoS<sub>2</sub> is enhanced as found in Figure 2(d).

The presence of the layer-sensitive Raman bands after thermal annealing strongly evidences that the MoS<sub>2</sub> and WSe<sub>2</sub> interact with each other. It is also possible that some contaminants such as adsorbates trapped between MoS<sub>2</sub> and WSe<sub>2</sub> weaken the coupling between these two layers. After the thermal treatment, these contaminants are efficiently removed (as indicated by AFM), thus resulting in the commensurate stacking and the shifts in the Raman peaks. Figure 2(e) is the OM for the selected area for Raman mapping studies. Figure 2(f) shows the spatial mappings for the peak intensity of the Raman bi-layer signature at 309 cm<sup>-1</sup> for WSe<sub>2</sub> A<sup>2</sup><sub>1g</sub> mode, and the Raman features is only observed and distributed uniformly in the stacked region, indicating that the peak is originated from the inter-layer coupling in the new MoS<sub>2</sub>/WSe<sub>2</sub> bilayer. It is noteworthy that the peak A<sup>2</sup><sub>1g</sub> is Raman inactive in monolayer but become active in homo-bilayer or thicker layers. Here, the heterojunction stacking likely introduces a similar effect as in stacked homo-layers, leading to the symmetry change and activation of the Raman features.

In order to further investigate the main features observed in the experimental Raman spectra of the MoS<sub>2</sub>/WSe<sub>2</sub> junction, density functional theory (DFT) and density functional perturbation theory (DFPT) calculations were carried out using the plane wave code CASTEP as implemented in the Materials Studio package.<sup>38</sup> A hexagonal unit cell with one layer of MoS<sub>2</sub> and another of WSe<sub>2</sub> arranged in an AB stacking was considered under the local density approximation (LDA). In order to provide a reasonable description of the van der Waals interaction, we have considered a dispersion correction for LDA (LDA-D).<sup>39</sup> After the relaxation, due to the lattice mismatch between the monolayers, the MoS<sub>2</sub> lattice parameter suffered an expansion from 3.16 to 3.21 Å and the WSe<sub>2</sub> lattice contracted from 3.28 to 3.21 Å. The phonon dispersion and Raman scattering modes were

calculated using the linear response approach for insulators.<sup>40</sup> The result of Raman scattering modes is shown in Figure 3, where all the modes, not the resonant second order or combinations of first order modes, are shown in the Figure 3. The characteristic peaks  $E'$  and  $A'_1$  for  $WSe_2$  and  $MoS_2$  are exactly reproduced. The  $MoS_2/WSe_2$  bilayer vibrations at  $309\text{ cm}^{-1}$  ( $WSe_2 A^2_{1g}$ ) is also clearly seen from the simulation. Although the calculated frequencies are not exactly the same as obtained in experiments, the simulation results provide a good approximation of the Raman signals observed. The coincidence between the experimental and simulated results implies that the coupling exists in the  $MoS_2/WSe_2$  bilayer heterojunction.

The Raman simulation in Figure 3 also presents the  $MoS_2$  bulk vibration mode  $A^2_{1g}$  at  $458\text{ cm}^{-1}$  and the anomaly  $E''$  mode at  $279\text{ cm}^{-1}$ . Comparing to our experimental results, although there have other Raman active modes near  $460\text{ cm}^{-1}$ , the  $MoS_2 A^2_{1g}$  mode still can be identified in Figure 2(d) for cW/M sample. The observed  $E''$  mode at  $284\text{ cm}^{-1}$  in Figure 2(b) for cW/M sample can also be correlated to the simulation result. This peak is not normally observed because of the Raman geometry used (back-scattering geometry) and also because it has low intensity. The observation on the  $E''$  mode may indicate the presence of the interlayer coupling could enhance its intensity. The observation on these Raman peaks for Bulk  $MoS_2$  is also an evidence of the existence of the interlayer coupling between  $MoS_2$  and  $WSe_2$ .

It is known that the Raman  $E'$  peak of monolayer  $MoS_2$  is sensitive to strain and strain could induce a red-shift in the  $E'$  modes that have been observed for  $MoS_2$  monolayer or multilayers in other reports.<sup>33, 41-43</sup> The red-shift of the  $MoS_2 E'$  peak after the two layers are coupled (thermally treated) shown in Figure 2(c) indicate that a tensile strain has been imposed to the  $MoS_2$ . This also implies that the  $WSe_2$  monolayer experiences a compressive strain and the  $E'$  peak of  $WSe_2$  also shows an opposite blue-shift as shown in Figure 2(a). As stated above, our simulation concludes the expansion of the  $MoS_2$  and contraction of the  $WSe_2$  (details in experimental section) which explain in part the  $E'$  peak shift in  $MoS_2$  and  $WSe_2$  after the two layers are coupled.

Although the strain effect could explain the Raman shifts of the annealed hetero bilayer, we still cannot exclude the possibility of charge transfer between these stacked layers. The Raman  $A'_1$  peak of  $MoS_2$  blue-shifts and its intensity increases (relative to  $E'$ ), thus indicating that  $MoS_2$  is less  $n$ -doped

(or a decrease in the electron concentration).<sup>44, 45</sup> The blue-shift of the WSe<sub>2</sub> Raman A'<sub>1</sub> peak implies that the WSe<sub>2</sub> may become less *p*-doped (Supporting Figure S3 shows that in our separate experiment, *p*-doping from AuCl<sub>4</sub><sup>-</sup> causes a red-shift of Raman A'<sub>1</sub> peak in monolayer WSe<sub>2</sub>). These phenomena suggest that the electrons transfer from MoS<sub>2</sub> to WSe<sub>2</sub>, which is expected for the PN-junction composed by the *p*-type WSe<sub>2</sub> and *n*-type MoS<sub>2</sub>.<sup>24-27</sup> It is also noted that the effect of a compressive strain on E' and the *n*-doping effect on A'<sub>1</sub> in WSe<sub>2</sub> is not easily distinguishable since A'<sub>1</sub> and E' frequencies in WSe<sub>2</sub> are degenerate and both effects are expected to cause the blue-shift. However, the fact that the Raman shift of MoS<sub>2</sub> E' mode is larger than the A'<sub>1</sub> mode implies that the strain effect should play a major role than doping effect. On the other hand, the theoretical simulation including only the strain relaxation can well reproduce our experimental results, which further suggests that the strain effect is more significant. In any case, the shifts indicate the interaction between two stacked heterolayers. It is worth noting that our results show that the A'<sub>1</sub> and E' peak energies of MoS<sub>2</sub> do not seem to depend on the stacking angle between the two layers as shown in Figure S4, which is different from the recent studies on Raman spectra of bilayer MoS<sub>2</sub> which shows twisting angle dependence.<sup>46, 47</sup> This could be reasoned since the homo-bilayer might exhibit stronger interlayer coupling due to the same lattice constant for two layers (better matching between top and bottom layers).

**Band Gaps and Band Alignments:** In order to study the optical and energy band properties of the hetero-junction, we performed the PL and absorption measurements. Figure 4(a) shows the PL spectra excited with a 532 nm laser and Figure 4(b) displays the absorption spectra for MoS<sub>2</sub>, un-coupled MoS<sub>2</sub>/WSe<sub>2</sub> hetero-junction (uM/W), coupled MoS<sub>2</sub>/WSe<sub>2</sub> hetero-junction (cM/W), and WSe<sub>2</sub> regions. The excitonic PL peaks for WSe<sub>2</sub> and MoS<sub>2</sub> monolayers at about 1.65 eV and 1.85 eV are clearly observed in the respective non-stacking region, and the peak energies also hold after annealing process as shown in Figure S2 (b). For the uM/W region, the PL peak energy of WSe<sub>2</sub> or MoS<sub>2</sub> is very close to that for its corresponding layer, thus confirming that there is no strong layer coupling in the hetero-junction. The slight suppression of the PL intensity for both MoS<sub>2</sub> and WSe<sub>2</sub>, may be due to the defects/traps introduced by the stacking. For the cM/W sample, the PL intensity for both WSe<sub>2</sub> and MoS<sub>2</sub> is significantly lower compared to that of uM/W. In addition to the characteristic PL peaks from



MoS<sub>2</sub> and WSe<sub>2</sub>, an extra peak at a lower energy (~1.59 eV), and marked by a black dashed line is also observed. This PL peak appeared in previous work and it is attributed to the inter-layer radiative recombination of the spatially separated carriers.<sup>27</sup> The excitons are excited separately in WSe<sub>2</sub> and MoS<sub>2</sub> by the incident laser. Since the MoS<sub>2</sub>/WSe<sub>2</sub> junction is a type II hetero-junction, the excited electrons in WSe<sub>2</sub> tend to accumulate in the conduction band of MoS<sub>2</sub> and the holes in MoS<sub>2</sub> in the valence band of WSe<sub>2</sub> at the interface as illustrated in Figure 5. Therefore, the recombination of the electron-hole pairs at the interface gives lower energy than MoS<sub>2</sub> and WSe<sub>2</sub> itself. The inter-layer PL peak reveals the nature of the coupling in the hetero-junction.

The absorption spectrum for individual MoS<sub>2</sub> exhibits two absorptions peaks, A and B excitonic peaks at 1.87 eV and 2.01 eV respectively. The WSe<sub>2</sub> has only one peak centered at 1.70 eV. As shown in Figure 4(b), the absorption peak of the pristine WSe<sub>2</sub> is significantly higher (50-60 meV) than that of either uW/M or cW/M, which might be due to that the WSe<sub>2</sub> is under MoS<sub>2</sub> and the dielectric environment is largely changed. Moreover, a Stoke shift is found in cM/W sample between absorption peak (1.64 eV) and inter-layer PL peak (1.59 eV), which further supports the radiative recombination between the WSe<sub>2</sub> and MoS<sub>2</sub>. We should note that we found an anti-Stoke shift in the cM/W sample between the WSe<sub>2</sub> absorption peak (1.64 eV) and WSe<sub>2</sub> PL peak (1.66 eV), as marked with orange lines in Figure 4. The anti-Stoke shift implies that there might have some hot phonons in the optical level of WSe<sub>2</sub> under the hetero-junction structure, which requires further experiments and theoretical work to clarify.

The observation on the inter-layer PL peak not only shows the strong evidence of the inter-layer coupling, but also allows us to establish the energy band alignment of the MoS<sub>2</sub>/WSe<sub>2</sub> hetero-junction and the exciton binding energy of the junction as shown in Figure 5. According to our previous work on STS<sup>28</sup> and  $\mu$ -XPS<sup>48</sup>, we know that the energy band gap for MoS<sub>2</sub> and WSe<sub>2</sub> are 2.34 eV and 2.46 eV, respectively, and the valence band offset is 0.42 eV. For consistency, we measure the PL spectrum at 77K to set the energy band alignment. The PL spectrum at 77K for each regime is shown in Figure S4, and the extracted PL peaks are summarized in Figure 5 with solid double arrow lines. Based on these, we can determine the exciton binding energy of the MoS<sub>2</sub>/WSe<sub>2</sub> inter-layer exciton, as marked by solid double arrow line with gray background.<sup>49-52</sup> We find that the MoS<sub>2</sub>/WSe<sub>2</sub> inter-layer exciton

has a lower exciton binding energy 0.26 eV when compared to MoS<sub>2</sub> or WSe<sub>2</sub>. The band alignment reveals the important role of the interlayer coupling, which is crucial for band engineering. In our work, we confirmed that the annealing process can enhance the interlayer coupling, which might result from reducing of layer distance or exclusion of interface residues in order to build novel van der Waals solids. Besides, we have also performed the experiments for the opposite stacking structure (WSe<sub>2</sub> on top of MoS<sub>2</sub>) and this structure exhibits the similar behaviors in Raman (Figures S5) and PL (Figure S6), further corroborating the conclusions reached.

## CONCLUSIONS

We fabricated the vertical MoS<sub>2</sub>/WSe<sub>2</sub> hetero-junction by stacking CVD-grown MoS<sub>2</sub> and WSe<sub>2</sub> triangular monolayers. The thermal treatment enhances the coupling between the two monolayers, based on the shifts observed in the Raman and PL spectra. Interestingly, the characteristic Raman signature at 309 cm<sup>-1</sup> (WSe<sub>2</sub> A<sup>2</sup><sub>1g</sub>), 463 cm<sup>-1</sup> (MoS<sub>2</sub> A<sup>2</sup><sub>1g</sub>), and 286 cm<sup>-1</sup> (MoS<sub>2</sub> E<sup>2</sup>) suggest that the hetero-structural stacking impose similar symmetry change as homo-structural stacking. Together with the reported STS and  $\mu$ -XPS results, the energy band alignment of the MoS<sub>2</sub>/WSe<sub>2</sub> hetero-junction and the exciton binding energy were established. It is anticipated that the fundamental understanding of interlayer coupling as well as the band alignments in hetero-structures are crucially important for future applications and engineering of the devices based on two-dimensional materials and van der Waals solids.

## METHODS

**WSe<sub>2</sub> / MoS<sub>2</sub> mono-layer single crystal growth:** WSe<sub>2</sub> and MoS<sub>2</sub> mono-layer single crystal were separately growth by chemical vapor deposit method. The WO<sub>3</sub> / MoO<sub>3</sub> powders (0.3 g / 0.6 g) were placed in a quartz boat located in the heating zone center of the furnace. The Se / S powders were placed in a separate quartz boat at the upper stream side of the furnace and the temperature was maintained at 290°C / 170°C during the reaction. The sapphire substrates for growing were put at the downstream side, next to quartz boat. The gas flow was brought by an Ar/H<sub>2</sub>/Ar flowing gas (Ar = 90 sccm, H<sub>2</sub> = 10 sccm / Ar = 70 sccm), and the chamber pressure was controlled at 7 Torr / 40 Torr. The

center heating zone was heated to 925°C / 635°C. After reaching growth temperature, the heating zone was kept for 15 / 30 minutes and the furnace was then naturally cooled down to room temperature.

***Hetero-junction fabrication:*** MoS<sub>2</sub> on sapphire substrate was spin-coated with PMMA (950K), and then heated on hot plate at 100°C for 20 minutes. The sample was then tipped into NaOH (2M) solution and kept at 100°C for 1 hour. After sapphire-etching by NaOH, MoS<sub>2</sub> with PMMA film was transferred into DI water twice, each step for 10 min, to dilute NaOH etching solution. And then MoS<sub>2</sub> with PMMA was transferred on sapphire with WSe<sub>2</sub> and heating at 100°C on hot plate for 30 minutes to evaporate the water at the interface. Following, the sample was put into Acetone at 60°C for 30 minutes to remove the PMMA. Finally, the sample was rinsing with IPA and water, and dried with N<sub>2</sub> gas. Before annealing, the samples were examined by AFM, Raman spectroscopy, PL, and absorption spectroscopy. The as-prepared MoS<sub>2</sub>/WSe<sub>2</sub> samples were then annealed in an hydrogen/Ar environment (atmosphere pressure; H<sub>2</sub>:Ar = 1:4) at 300°C for 4hr. The annealing temperature was selected at 300°C to effectively remove the residuals but not too high to initiate the formation of alloys such as MoS<sub>x</sub>Se<sub>y</sub> or WS<sub>x</sub>Se<sub>y</sub>.<sup>49</sup>

***Characterizations:*** The AFM images were performed in a Veeco Dimension-Icon system. Raman spectra were collected in a confocal Raman system (NT-MDT). The wavelength of laser is 473 nm (2.63eV), and the spot size of the laser beam is ~0.5μm and the spectral resolution is 1 cm<sup>-1</sup> (obtained with a 1800 grooves/mm grating). The PL and differential reflectance spectra were measured in a home-made microscopy system. For room-temperature PL measurements, a 532 nm solid-state laser was focused to a spot size < 1 μm on the sample by an objective lens (×100; N.A.= 0.9). The PL signals were then collected by the same objective lens, analyzed by a 0.75 m monochromator and detected by a liquid-nitrogen-cooled CCD camera. The apparatus for the differential reflectance measurements are basically the same, except that the light source was replaced by a fiber-coupled tungsten-halogen lamp. For low-temperature PL measurements, the sample was cooled down to  $T = 10.8\text{K}$  in a low-vibration cryogen-free cryostat. The objective lens for low-temperature measurements is a long working distance objective lens with N.A. = 0.42.

***Phonon dispersion and Raman scattering modes simulation:*** The density functional theory (DFT) and density functional perturbation theory (DFPT) calculations were carried using the plane wave code CASTEP<sup>38</sup> as implemented in the Materials Studio package. A hexagonal unit cell with one layer of MoS<sub>2</sub> and another of WSe<sub>2</sub> arranged in a AB stacking (similar to the one observed in bulk crystals of trigonal prismatic transition metal dichalcogenides) was considered under the local density approximation (LDA) using the Ceperly-Alder-Perdew and Zunger (CA-PZ) functional<sup>54, 55</sup> with 6X6X3 Monkhorst-Pack K-points and a plane waves cut off of 720 eV with a norm-conserving pseudopotential. The structure was relaxed, including the cell, until the forces became smaller than 0.01 eV/Å and with self-consistent energy tolerances less than  $5 \times 10^{-7}$  eV/atom. A vacuum of 16 Å between the cells was considered. The electronic structure results obtained for the individual layers and bulk are in agreement with those reported by other groups within the LDA formalism.<sup>56, 57</sup> In order to provide a reasonable description of the van der Waals interaction, we have considered a dispersion correction for both LDA (LDA-D)<sup>39</sup> and for general gradient approximation (GGA-PW91)<sup>58</sup> finding that LDA provides a better description for the interlayer distance than LDA-D and corrected GGA-PW91, as described in a previous publications.<sup>35, 59</sup> The phonon dispersion and Raman scattering modes were calculated using the linear response approach for insulators<sup>40</sup>. After the relaxation, due to the lattice mismatch between the monolayers, the MoS<sub>2</sub> lattice parameter suffered an expansion from 3.16 to 3.21 Å and the WSe<sub>2</sub> lattice contracted from 3.28 to 3.21 Å. The expansion of the MoS<sub>2</sub> and contraction of the WSe<sub>2</sub> explain in part the shifts in some of the modes found in the Raman signal due to strain. Nevertheless, the results obtained here provide a good approximation of the Raman signal observed.

#### **ACKNOWLEDGMENTS:**

This research was partly supported by National Science Council Taiwan (NSC-102-2119-M-001-005-MY3 and NSC101-2628-M-009-002-MY3) and AFOSR BRI. WHC acknowledges the supports from the Center for Interdisciplinary Science under the MOE-ATU project for NCTU. MHC and LJL acknowledge the supports from KAUST. MT acknowledges support by the U. S. Army Research

Office under MURI ALNOS project, contract/grant number W911NF-11-1-0362, the Penn State Center for Nanoscale Science (seed grant on 2D Layered Materials -DMR-0820404), and the Center for 2-Dimensional and Layered Materials at The Pennsylvania State University.

**Supporting Information Available:** Figures S1-S4 are included. This material is available free of charge *via* the Internet at <http://pubs.acs.org>.

## REFERENCES

1. Lee, Y.-H.; Zhang, X.-Q.; Zhang, W.; Chang, M.-T.; Lin, C.-T.; Chang, K.-D.; Yu, Y.-C.; Wang, J. T.-W.; Chang, C.-S.; Li, L.-J., *et al.* Synthesis of Large-Area MoS<sub>2</sub> Atomic Layers with Chemical Vapor Deposition. *Adv. Mater.* **2012**, 24, 2320-2325.
2. Huang, J.-K.; Pu, J.; Hsu, C.-L.; Chiu, M.-H.; Juang, Z.-Y.; Chang, Y.-H.; Chang, W.-H.; Iwasa, Y.; Takenobu, T.; Li, L.-J. Large-Area Synthesis of Highly Crystalline WSe<sub>2</sub> Monolayers and Device Applications. *ACS Nano* **2013**, 8, 923-930.
3. Lin, Y.-C.; Zhang, W.; Huang, J.-K.; Liu, K.-K.; Lee, Y.-H.; Liang, C.-T.; Chu, C.-W.; Li, L.-J. Wafer-scale MoS<sub>2</sub> Thin Layers Prepared by MoO<sub>3</sub> Sulfurization. *Nanoscale* **2012**, 4, 6637-6641.
4. Mak, K. F.; Lee, C.; Hone, J.; Shan, J.; Heinz, T. F. Atomically Thin MoS<sub>2</sub>: A New Direct-Gap Semiconductor. *Phys. Rev. Lett.* **2010**, 105, 136805.
5. Ramasubramaniam, A. Large Excitonic Effects in Monolayers of Molybdenum and Tungsten Dichalcogenides. *Phys. Rev. B* **2012**, 86, 115409.
6. Lee, C.; Yan, H.; Brus, L. E.; Heinz, T. F.; Hone, J.; Ryu, S. Anomalous Lattice Vibrations of Single- and Few-Layer MoS<sub>2</sub>. *ACS Nano* **2010**, 4, 2695-2700.
7. Jones, A. M.; Yu, H.; Ghimire, N. J.; Wu, S.; Aivazian, G.; Ross, J. S.; Zhao, B.; Yan, J.; Mandrus, D. G.; Xiao, D., *et al.* Optical Generation of Excitonic Valley Coherence in Monolayer WSe<sub>2</sub>. *Nat Nanotechnol.* **2013**, 8, 634-638.
8. Splendiani, A.; Sun, L.; Zhang, Y.; Li, T.; Kim, J.; Chim, C.-Y.; Galli, G.; Wang, F. Emerging Photoluminescence in Monolayer MoS<sub>2</sub>. *Nano Lett.* **2010**, 10, 1271-1275.
9. Wang, Q. H.; Kalantar-Zadeh, K.; Kis, A.; Coleman, J. N.; Strano, M. S. Electronics and Optoelectronics of Two-dimensional Transition Metal Dichalcogenides. *Nat. Nanotechnol.* **2012**, 7, 699-712.
10. Wang, H.; Yu, L.; Lee, Y.-H.; Shi, Y.; Hsu, A.; Chin, M. L.; Li, L.-J.; Dubey, M.; Kong, J.; Palacios, T. Integrated Circuits Based on Bilayer MoS<sub>2</sub> Transistors. *Nano Lett.* **2012**, 12, 4674-4680.
11. Radisavljevic, B.; Radenovic, A.; Brivio, J.; Giacometti, V.; Kis, A. Single-layer MoS<sub>2</sub> transistors. *Nat. Nanotechnol.* **2011**, 6, 147-150.
12. Radisavljevic, B.; Whitwick, M. B.; Kis, A. Small-signal amplifier based on single-layer MoS<sub>2</sub>. *Appl. Phys. Lett.* **2012**, 101, 043103.

13. Fang, H.; Chuang, S.; Chang, T. C.; Takei, K.; Takahashi, T.; Javey, A. High-Performance Single Layered WSe<sub>2</sub> p-FETs with Chemically Doped Contacts. *Nano Lett.* **2012**, 12, 3788-3792.
14. Lee, Y.-H.; Yu, L.; Wang, H.; Fang, W.; Ling, X.; Shi, Y.; Lin, C.-T.; Huang, J.-K.; Chang, M.-T.; Chang, C.-S., *et al.* Synthesis and Transfer of Single-Layer Transition Metal Disulfides on Diverse Surfaces. *Nano Lett.* **2013**, 13, 1852-1857.
15. Zhang, W.; Chuu, C.-P.; Huang, J.-K.; Chen, C.-H.; Tsai, M.-L.; Chang, Y.-H.; Liang, C.-T.; Chen, Y.-Z.; Chueh, Y.-L.; He, J.-H., *et al.* Ultrahigh-Gain Photodetectors Based on Atomically Thin Graphene-MoS<sub>2</sub> Heterostructures. *Sci. Rep.* **2014**, 4, 3826.
16. Bertolazzi, S.; Krasnozhon, D.; Kis, A. Nonvolatile Memory Cells Based on MoS<sub>2</sub>/Graphene Heterostructures. *ACS Nano* **2013**, 7, 3246-3252.
17. Britnell, L.; Gorbachev, R. V.; Jalil, R.; Belle, B. D.; Schedin, F.; Mishchenko, A.; Georgiou, T.; Katsnelson, M. I.; Eaves, L.; Morozov, S. V., *et al.* Field-Effect Tunneling Transistor Based on Vertical Graphene Heterostructures. *Science* **2012**, 335, 947-950.
18. Geim, A. K.; Grigorieva, I. V. Van der Waals Heterostructures. *Nature* **2013**, 499, 419-425.
19. Sup Choi, M.; Lee, G.-H.; Yu, Y.-J.; Lee, D.-Y.; Hwan Lee, S.; Kim, P.; Hone, J.; Jong Yoo, W. Controlled Charge Trapping by Molybdenum Disulphide and Graphene in Ultrathin Heterostructured Memory Devices. *Nat. Commun.* **2013**, 4, 1624.
20. Georgiou, T.; Jalil, R.; Belle, B. D.; Britnell, L.; Gorbachev, R. V.; Morozov, S. V.; Kim, Y.-J.; Gholinia, A.; Haigh, S. J.; Makarovskiy, O., *et al.* Vertical Field-effect Transistor based on Graphene-WS<sub>2</sub> Heterostructures for Flexible and Transparent Electronics. *Nat. Nanotechnol.* **2013**, 8, 100-103.
21. Britnell, L.; Ribeiro, R. M.; Eckmann, A.; Jalil, R.; Belle, B. D.; Mishchenko, A.; Kim, Y.-J.; Gorbachev, R. V.; Georgiou, T.; Morozov, S. V., *et al.* Strong Light-Matter Interactions in Heterostructures of Atomically Thin Films. *Science* **2013**, 340, 1311-1314.
22. Haigh, S. J.; Gholinia, A.; Jalil, R.; Romani, S.; Britnell, L.; Elias, D. C.; Novoselov, K. S.; Ponomarenko, L. A.; Geim, A. K.; Gorbachev, R. Cross-sectional Imaging of Individual Layers and Buried Interfaces of Graphene-based Heterostructures and Superlattices. *Nat. Mater.* **2012**, 11, 764-767.
23. Rivera, P.; Schaibley, J. R.; Jones, A. M.; Ross, J. S.; Wu, S.; Aivazian, G.; Klement, P.; Ghimire, N. J.; Yan, J.; Mandrus, D. G., *et al.*, Observation of Long-Lived Interlayer Excitons in Monolayer MoSe<sub>2</sub>-WSe<sub>2</sub> Heterostructures. *ArXiv*: 1403. 4985, **2014**.
24. Cheng, R.; Li, D.; Zhou, H.; Wang, C.; Yin, A.; Jiang, S.; Liu, Y.; Chen, Y.; Huang, Y.; Duan, X., Electroluminescence and Photocurrent Generation from Atomically Sharp WSe<sub>2</sub>/MoS<sub>2</sub> Heterojunction p-n Diodes. *ArXiv*: 1403. 3447, **2014**.
25. Furchi, M. M.; Pospischil, A.; Libisch, F.; Burgdorfer, J.; Mueller, T., Photovoltaic Effect in an Electrically Tunable van der Waals Heterojunction. *ArXiv*: 1403. 2652, **2014**.
26. Lee, C.-H.; Lee, G.-H.; van der Zande, A. M.; Chen, W.; Li, Y.; Han, M.; Cui, X.; Arefe, G.; Nuckolls, C.; Heinz, T. F., *et al.*, Atomically Thin p-n Junctions with van der Waals Heterointerfaces. *ArXiv*: 1403. 3062, **2014**.
27. Fang, H.; Battaglia, C.; Carraro, C.; Nemsak, S.; Ozdol, B.; Kang, J. S.; Bechtel, H. A.; Desai, S. B.; Kronast, F.; Unal, A. A., *et al.* Strong Interlayer Coupling in van der Waals Heterostructures Built from Single-Layer Chalcogenides. *Proc. Natl. Acad. Sci. U. S. A.* **2014**, 111, 6198-6202.

28. Zhang, C.; Johnson, A.; Hsu, C. L.; Li, L. J.; Shih, C. K. Direct Imaging of Band Profile in Single Layer MoS<sub>2</sub> on Graphite: Quasiparticle Energy Gap, Metallic Edge States, and Edge Band Bending. *Nano Lett.* **2014**, *14*, 2443-2447.
29. Luo, X.; Zhao, Y.; Zhang, J.; Toh, M.; Kloc, C.; Xiong, Q.; Quek, S. Y. Effects of lower symmetry and dimensionality on Raman spectra in two-dimensional WSe<sub>2</sub>. *Phys. Rev. B* **2013**, *88*, 195313.
30. Tonndorf, P.; Schmidt, R.; Böttger, P.; Zhang, X.; Börner, J.; Liebig, A.; Albrecht, M.; Kloc, C.; Gordan, O.; Zahn, D. R. T., *et al.* Photoluminescence Emission and Raman Response of Monolayer MoS<sub>2</sub>, MoSe<sub>2</sub>, and WSe<sub>2</sub>. *Opt. Express* **2013**, *21*, 4908-4916.
31. Molina-Sánchez, A.; Wirtz, L. Phonons in Single-layer and Few-layer MoS<sub>2</sub> and WS<sub>2</sub>. *Phys. Rev. B* **2011**, *84*, 155413.
32. Wieting, T. J.; Verble, J. L. Infrared and Raman Studies of Long-Wavelength Optical Phonons in Hexagonal MoS<sub>2</sub>. *Phys. Rev. B* **1971**, *3*, 4286-4292.
33. Rice, C.; Young, R. J.; Zan, R.; Bangert, U.; Wolverson, D.; Georgiou, T.; Jalil, R.; Novoselov, K. S. Raman-Scattering Measurements and First-Principles Calculations of Strain-induced Phonon Shifts in Monolayer MoS<sub>2</sub>. *Phys. Rev. B* **2013**, *87*, 081307.
34. Li, H.; Zhang, Q.; Yap, C. C. R.; Tay, B. K.; Edwin, T. H. T.; Olivier, A.; Baillargeat, D. From Bulk to Monolayer MoS<sub>2</sub>: Evolution of Raman Scattering. *Adv. Funct. Mater.* **2012**, *22*, 1385-1390.
35. Terrones, H.; Corro, E. D.; Feng, S.; Poumirol, J. M.; Rhodes, D.; Smirnov, D.; Pradhan, N. R.; Lin, Z.; Nguyen, M. A. T.; Elias, A. L., *et al.* New First Order Raman-active Modes in Few Layered Transition Metal Dichalcogenides. *Sci. Rep.* **2014**, *4*, 4215.
36. Zhang, X.; Han, W. P.; Wu, J. B.; Milana, S.; Lu, Y.; Li, Q. Q.; Ferrari, A. C.; Tan, P. H. Raman Spectroscopy of Shear and Layer Breathing Modes in Multilayer MoS<sub>2</sub>. *Phys. Rev. B* **2013**, *87*, 115413.
37. Zhao, W.; Ghorannevis, Z.; Amara, K. K.; Pang, J. R.; Toh, M.; Zhang, X.; Kloc, C.; Tan, P. H.; Eda, G. Lattice Dynamics in Mono- and Few-layer Sheets of WS<sub>2</sub> and WSe<sub>2</sub>. *Nanoscale* **2013**, *5*, 9677-9683.
38. Clark, S. J.; Segall, M. D.; Pickard, C. J.; Hasnip, P. J.; Probert, M. J.; Refson, K.; Payne, M. C. First Principles Methods using CASTEP. *Z. Kristallogr.* **2005**, *220*, 567-570.
39. Ortman, F.; Bechstedt, F.; Schmidt, W. G. Semiempirical van der Waals Correction to the Density Functional Description of Solids and Molecular Structures. *Phys. Rev. B* **2006**, *73*, 205101.
40. Refson, K.; Tulip, P. R.; Clark, S. J. Variational Density-Functional Perturbation Theory for Dielectrics and Lattice Dynamics. *Phys. Rev. B* **2006**, *73*, 155114.
41. Wang, Y.; Cong, C.; Qiu, C.; Yu, T. Raman Spectroscopy Study of Lattice Vibration and Crystallographic Orientation of Monolayer MoS<sub>2</sub> under Uniaxial Strain. *Small* **2013**, *9*, 2857-2861.
42. Castellanos-Gomez, A.; Roldán, R.; Cappelluti, E.; Buscema, M.; Guinea, F.; van der Zant, H. S. J.; Steele, G. A. Local Strain Engineering in Atomically Thin MoS<sub>2</sub>. *Nano Lett.* **2013**, *13*, 5361-5366.

43. Zhu, C. R.; Wang, G.; Liu, B. L.; Marie, X.; Qiao, X. F.; Zhang, X.; Wu, X. X.; Fan, H.; Tan, P. H.; Amand, T., et al. Strain Tuning of Optical Emission Energy and Polarization in Monolayer and Bilayer MoS<sub>2</sub>. *Phys. Rev. B* **2013**, 88, 121301.
44. Shi, Y.; Huang, J.-K.; Jin, L.; Hsu, Y.-T.; Yu, S. F.; Li, L.-J.; Yang, H. Y. Selective Decoration of Au Nanoparticles on Monolayer MoS<sub>2</sub> Single Crystals. *Sci. Rep.* **2013**, 3, 1839.
45. Chakraborty, B.; Bera, A.; Muthu, D. V. S.; Bhowmick, S.; Waghmare, U. V.; Sood, A. K. Symmetry-dependent Phonon Renormalization in Monolayer MoS<sub>2</sub> transistor. *Phys. Rev. B* **2012**, 85, 161403.
46. Liu, K.; Zhang, L.; Cao, T.; Jin, C.; Qiu, D.; Zhou, Q.; Zettl, A.; Yang, P.; Louie, S. G.; Wang, F., Evolution of Interlayer Coupling in Twisted MoS<sub>2</sub> Bilayers. *ArXiv*: 1406. 6487, **2014**.
47. van der Zande, A. M.; Kunstmann, J.; Chernikov, A.; Chenet, D. A.; You, Y.; Zhang, X.; Huang, P. Y.; Berkelbach, T. C.; Wang, L.; Zhang, F., et al. Tailoring the Electronic Structure in Bilayer Molybdenum Disulfide via Interlayer Twist. *Nano Lett.* **2014**, 14, 3869-3875.
48. Chiu, M.-H.; Zhang, C.; Shiu, H. W.; Chuu, C.-P.; Chen, C.-H.; Chang, C.-Y. S.; Chen, C.-H.; Chou, M.-Y., et al., Determination of Band Alignment in Transition Metal Dichalcogenides Heterojunctions. *ArXiv*:1406. 5137, **2014**.
49. Su, S.-H.; Hsu, W.-T.; Hsu, C.-L.; Chen, C.-H.; Chiu, M.-H.; Lin, Y.-C.; Chang, W.-H.; Suenaga, K.; He, J.-H.; Li, L.-J. Controllable Synthesis of Band Gap-Tunable and Monolayer Transition Metal Dichalcogenide Alloys. *Frontiers in Energy Research* **2014**, 2, 27.
50. Ramasubramaniam, A., Large Excitonic effect in Monolayer of Molybdenum and Tungsten Dichalcogenides. *Phys. Rev. B* **2012**, 86, 115409
51. Klots, A. R.; Newaz, A. K. M.; Wang, B.; Prasai, D.; Krzyzanowska, H.; Caudel, D.; Ghimire, N. J.; Yan, J.; Ivanov, B. L.; Velizhanin, K. A., et al., Probing Excitonic States in Ultraclean Suspended Two-dimensional Semiconductors by Photocurrent Spectroscopy. *ArXiv*:1403. 6455, **2014**.
52. H. Shi, H. Pan, Y.-W. Zhang, and B. I. Yakobson, Quasiparticle Band Structures and Optical Properties of Strained Monolayer MoS<sub>2</sub> and WS<sub>2</sub>, *Phys. Rev. B* **2013**, 87, 155304.
53. Liang, Y.; Huang, S.; Soklaski, R.; Yang, L. Quasiparticle Band-edge Energy and Band Offsets of Monolayer of Molybdenum and Tungsten Chalcogenides. *Applied Physics Letters* **2013**, 103, 042106.
54. Ceperley, D. M.; Alder, B. J. Ground-State of The Electron-Gas by a Stochastic Method. *Phys. Rev. Lett.* **1980**, 45, 566-569.
55. Perdew, J. P.; Zunger, A. Self-Interaction Correction to Density-Functional Approximations for Many-Electron Systems. *Phys. Rev. B* **1981**, 23, 5048-5079.
56. Ding, Y.; Wang, Y.; Ni, J.; Shi, L.; Shi, S.; Tang, W. First Principles Study of Structural, Vibrational and Electronic Properties of Graphene-like MX<sub>2</sub> (M=Mo, Nb, W, Ta; X=S, Se, Te) Monolayers. *Physica B* **2011**, 406, 2254-2260.
57. Mahatha, S. K.; Patel, K. D.; Menon, K. S. R. Electronic Structure Investigation of MoS<sub>2</sub> and MoSe<sub>2</sub> using Angle-resolved Photoemission Spectroscopy and *ab initio* Band Structure Studies. *J. Phys. Condens. Matter* **2012**, 24, 475504.
58. Perdew, J. P.; Chevary, J. A.; Vosko, S. H.; Jackson, K. A.; Pederson, M. R.; Singh, D. J.;



Fiolhais, C. Atoms, Molecules, Solids, And Surfaces: Applications of the Generalized Gradient Approximation for the Exchange and Correlation. *Phys. Rev. B* **1992**, 46, 6671-6687.

59. Terrones, H.; Lopez-Urias, F.; Terrones, M. Novel Hetero-Layered Materials with Tunable Direct Band Gaps by Sandwiching Different Metal Disulfides and Diselenides. *Sci. Rep.* **2013**, 3, 1549.

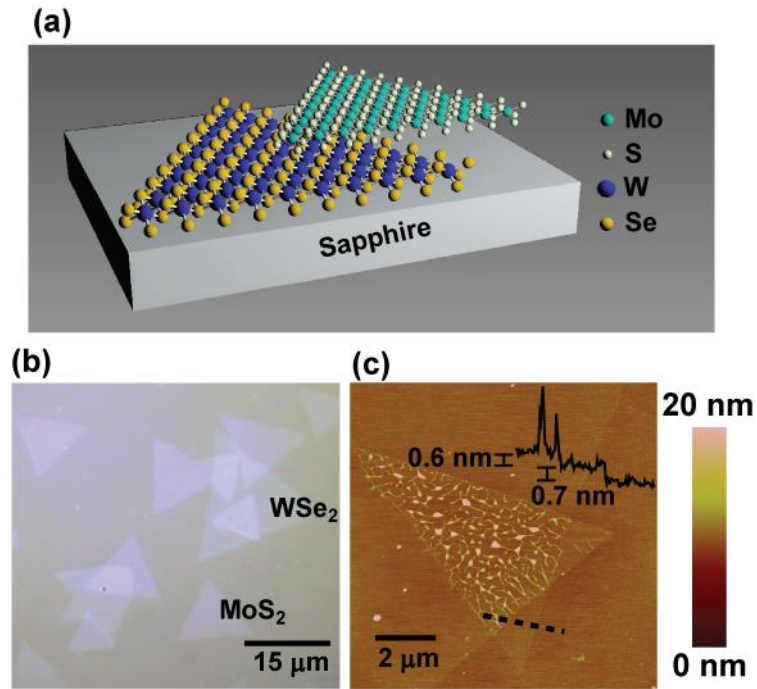


**Figure 1.** Representation of the vertical hetero-junction consisting of MoS<sub>2</sub> monolayers deposited on top of WSe<sub>2</sub> monolayers: (a) Schematic illustration of the MoS<sub>2</sub>/WSe<sub>2</sub> van der Waals hetero-junction; (b) Optical micrograph of the mechanically stacked MoS<sub>2</sub>/WSe<sub>2</sub> structure after thermal annealing, and (c) AFM image of the MoS<sub>2</sub>/WSe<sub>2</sub> hetero-junction. The cross-sectional height profile along the dashed line indicates that each layer is about 0.6~0.7 nm in thickness.

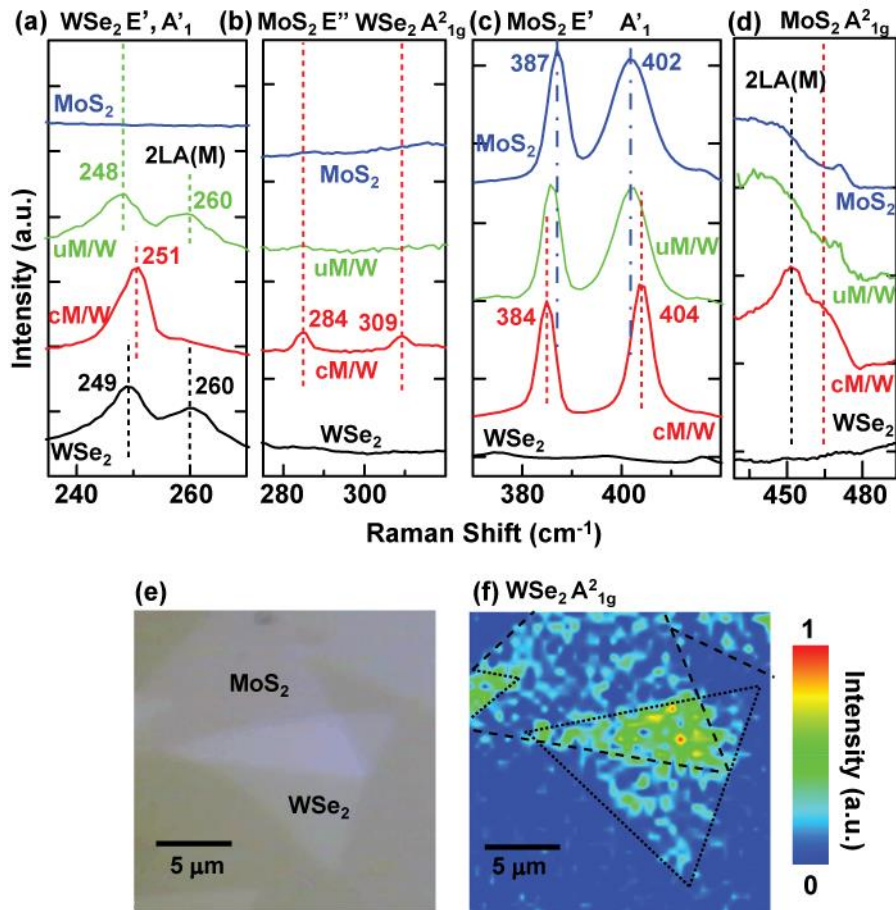


**Figure 2.** Raman spectra of the MoS<sub>2</sub>/WSe<sub>2</sub> hetero-junction. (a)-(d) Raman spectra for MoS<sub>2</sub> (blue), un-coupled MoS<sub>2</sub>/WSe<sub>2</sub> hetero-junction (green; uM/W), coupled MoS<sub>2</sub>/WSe<sub>2</sub> hetero-junction (red; cM/W), and WSe<sub>2</sub> (black) from the top to the bottom plot. The curves are shift for clarity. (e) Optical microscopic image for the MoS<sub>2</sub>/WSe<sub>2</sub> hetero-junction. (f) The spatial mapping of the Raman intensity for WSe<sub>2</sub> A<sub>2</sub><sup>1g</sup> peak in the selected area shown in (e).

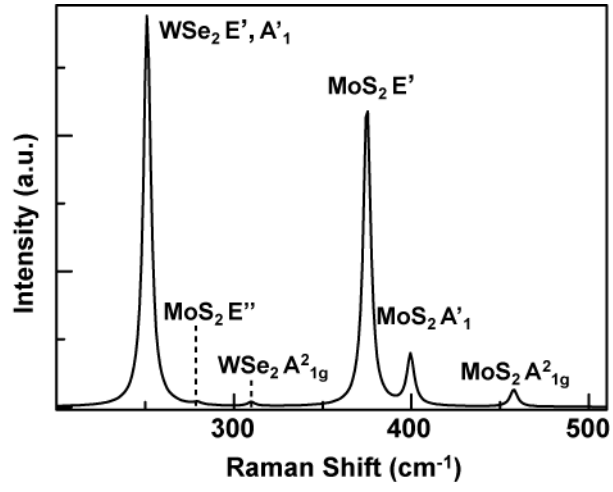


**Figure 3.** The Raman scattering modes simulation of the MoS<sub>2</sub>/WSe<sub>2</sub> hetero-junction.

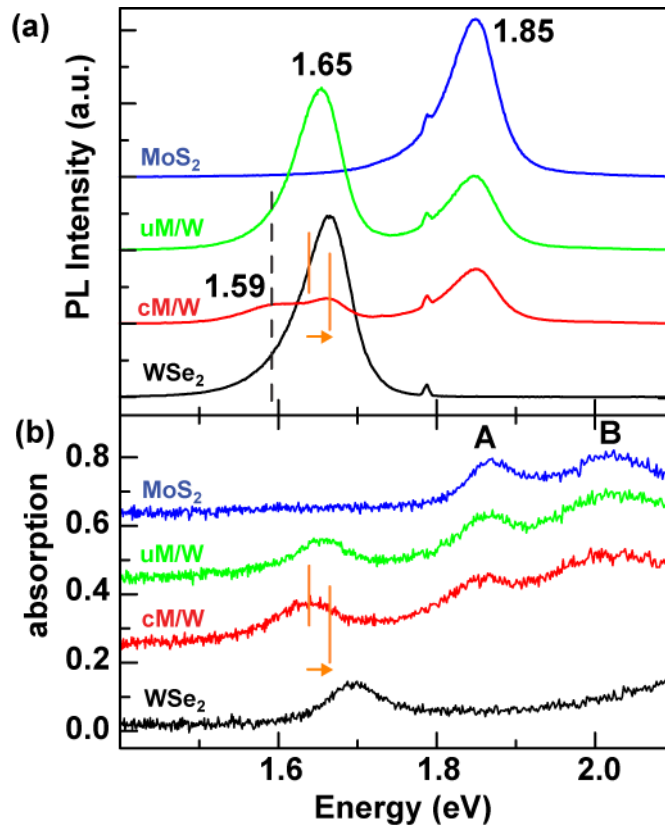


**Figure 4.** (a) Photoluminescence and (b) absorption spectroscopy of the MoS<sub>2</sub>/WSe<sub>2</sub> hetero-junction. The curves corresponding to MoS<sub>2</sub> (blue), non-coupled MoS<sub>2</sub>/WSe<sub>2</sub> hetero-junction (uM/W) (green), coupled MoS<sub>2</sub>/WSe<sub>2</sub> hetero-junction (cM/W) (red), and WSe<sub>2</sub> (black) from up to down. The curves are shift for clarity. The dashed line indicates the interlayer PL peak. The orange lines and arrow mark the anti-Stoke shift.

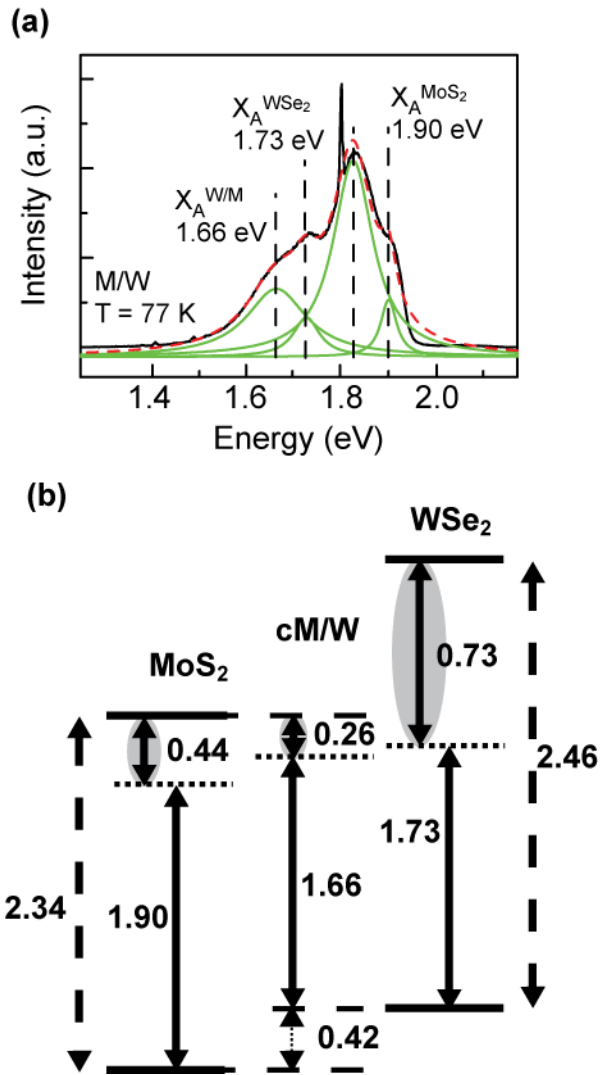


**Figure 5.** Schematic of the energy band alignment of MoS<sub>2</sub>/WSe<sub>2</sub> hetero-junction at 77K. (a) The PL of cM/W sample (black) and the Lorentzian peaks fitting (red-dashed) at 77K. The green lines are the composed peaks by using Lorentzian fitting. The black dashed lines indicate the emitted energy of MoS<sub>2</sub> and WSe<sub>2</sub> and cM/W. (b) The solid lines represent the conduction band and valence band of MoS<sub>2</sub> and WSe<sub>2</sub>. The solid double arrow lines, dashed double arrow lines, and dot double arrow lines indicate the PL energy, band gap energy, and the valence band offset between MoS<sub>2</sub> and WSe<sub>2</sub> extracted from experimental results, respectively. The solid double arrow lines with gray background indicate the derived exciton binding energy.